JOURNAL OF PROPULSION AND POWER
Vol. 13, No. 1, January–February 1997

Numerical Study of Hypervelocity Flows Through a Scramjet Combustor

R. Krishnamurthy*
North Carolina A&T State University, Greensboro, North Carolina 27411
R. C. Rogers†
NASA Langley Research Center, Hampton, Virginia 23681
and
S. N. Tiwari‡
Old Dominion University, Norfolk, Virginia 23529

Results are reported from a numerical investigation of mixing and combustion of hydrogen injected into an airstream at high enthalpy (flight Mach number 17). Numerical computations performed using the general aerodynamic simulation program code are compared with experimental data obtained with a rectangular combustor model in the free-piston driven, reflected-shock tunnel facility T5, at the Graduate Aeronautical Laboratories at the California Institute of Technology. Computed results show good agreement with the measured static wall pressures. Mixing performance with the injection of hot hydrogen is shown to be in line with established correlations for scramjet design. Also, the issue of spatial uniformity of the hydrogen–air mixture has been explored.

Nomenclature

A_c = area of cross section
$\bar{C}$ = average of C_i over a cross-sectional plane
C_i = local concentration of hydrogen
$C_{\rm rms}$ = rms deviation of C_i from $\bar{C}$
f = stoichiometric fuel–air (mass) ratio
M = Mach number
$\tilde{M}$ = molecular weight
$\dot{m}_R$ = axial mass flow rate of the least available reactant
N = total number of computational cells in the crossflow plane
P = static pressure
R = ratio of dynamic pressure of fuel jet to that of the airstream
T_t = stagnation temperature
u = velocity component in the x direction
x = direction along the length of the combustor (principal flow direction)
Y_R = mass fraction of the least available reactant
y = direction perpendicular to x in the plane of the injection wall
z = direction perpendicular to the plane of the injection wall
η_c = combustion efficiency
η_m = mixing efficiency
ρ = density
ϕ = fuel–air equivalence ratio

Subscripts
f = fuel
in = inflow

Presented as Paper 94-0773 at the AIAA 32nd Aerospace Sciences Meeting and Exhibit, Reno, NV, Jan. 10–13, 1994; received May 27, 1994; revision received Jan. 10, 1996; accepted for publication April 26, 1996.

*Research Staff, NASA Center of Research Excellence. Member AIAA.
†Senior Research Engineer, Hypersonic Air Breathing Propulsion Branch. Senior Member AIAA.
‡Eminent Professor, Department of Mechanical Engineering. Associate Fellow AIAA.

Introduction

INTEREST in high-speed, air-breathing propulsion systems such as scramjets, has been revived in recent years as a result of the National Aerospace Plane (NASP) program. The objective of the NASP program is to develop a vehicle capable of transatmospheric flight. The Mach number level within the engine/combustor of such a vehicle is rather high ($M > 5$). Ground-based testing of such scramjet engines requires a facility that cannot only achieve the proper Mach number, but also provides the proper pressures and temperatures to simulate the combustion processes. At present, only pulse-type facilities can provide such high-enthalpy flows. The newest of these is the free-piston driven, reflected shock tunnel, T5 located at the Graduate Aeronautical Laboratories at the California Institute of Technology (GALCIT).[1] Another such pulse facility currently in use in the U.S. is the NASA HYPULSE expansion tube located at General Applied Science Laboratory (GASL) Inc.[2] A new free-piston driven facility, the G-Range Impulse facility at the Arnold Engineering Development Center (AEDC) is being constructed.[3]

In all of these pulse facilities, high enthalpy levels are generated by heating the test gas with a shock wave. In T5 and the G-Range Impulse facility, the test gas undergoes a steady expansion through a contoured nozzle. Also, both employ free-piston drivers, with the piston in the G-Range Impulse Facility being expendable. The expansion tube uses an unsteady expansion in a constant-area tube to generate the high enthalpy. An expansion tube has a limited test time (0.5 ms) and thus the length of the models that can be tested is smaller. In contrast, the reflected shock tunnel allows for longer test times (1–2 ms), but the test gas is more dissociated than that in an expansion tube. The presence of significant levels of dissociated test gas in free-piston shock tunnels complicates the interpretation of test results in relation to the actual flight conditions where the air is not dissociated.

Recently, a generic combustor model was tested in T5 and the experimental data from that investigation are analyzed in the present study. The principal aim of this study is to analyze

Table 1 Main flow conditions in T5

	Low pressure		High pressure	
Test gas	Air	Nitrogen	Air	Nitrogen
Reservoir conditions				
Stagnation pressure, MPa	37.5	37.5	85.0	85.0
Stagnation temperature, K	7860	8476	8100	8875
Stagnation enthalpy, MJ/kg	15.3	15.3	15.4	15.7
Test section conditions				
Temperature, K	2125	2015	2340	2210
Pressure, kPa	18.3	16.8	43.9	38.5
Density, kg/m^3	0.028	0.027	0.063	0.058
Velocity, m/s	4785	4885	4805	5005
Mach number	5.26	5.54	5.17	5.45
Concentration, mass fractions				
O_2	0.1211	——	0.1560	——
O	0.0839	——	0.0470	——
NO	0.0514	——	0.0560	——

Table 2 Hydrogen injection conditions

T5 pressure conditions,	Low pressure			High pressure	
hydrogen injection	Cold	Cold	Hot	Hot	Hot
Injection conditions					
Stagnation pressure, MPa	0.41	0.79	1.5	2.4	4.8
Stagnation temperature, K	300	300	1250	1500	1500
Exit pressure, kPa	83	160	305	485	970
Exit temperature, K	190	190	790	950	950
Exit velocity, m/s	1780	1780	3640	3980	3980
ϕ	1.0	1.9	1.8	1.1	2.2
R, $R = (\rho U^2)_{jet}/(\rho U^2)_{inlet}$	0.52	1.01	1.94	1.35	2.70

the available experimental data by using an existing computational fluid dynamics (CFD) tool, and then to use the computed solutions to investigate the performance characteristics of the fuel injection method using mixing and combustion efficiencies.

Facility, Model, and Data

The design of the T5 facility at GALCIT has evolved from the experience gained in the operation of a number of free-piston driven tunnels since the 1960s. The T5 facility can be used to study hypervelocity ($M > 10$) flows with freestream velocity levels up to 6 km/s.

The free piston in T5, which is driven by compressed air, compresses and heats the helium driver gas to a state at which the main diaphragm bursts. The normal shock that results compresses the test gas (air or nitrogen) in the driven tube. When this primary shock reaches the end of the driven tube, a reflected shock is formed that stagnates the flow of the test gas and causes the secondary diaphragm to burst. The test gas then expands into the test section through a contoured nozzle to the desired operating conditions. Steady flow conditions in the test section exist for about 1–2 ms. A detailed description of the operational characteristics of T5 is given by Hornung.[1]

At the end of the driven section, where the reflected shock stagnates the flow, the test gas reaches a temperature of nearly 9000 K and a pressure of 70 MPa. Under these conditions, the nitrogen and oxygen molecules dissociate. As the flow expands through the nozzle, the temperature decreases, resulting in some recombination of the dissociated molecules. However, because of the high velocities and low density levels in the nozzle, the recombination rates are usually insufficient to maintain equilibrium molecular composition. The result is a test gas with significant levels of dissociated oxygen and nitrogen. The HYPULSE expansion tube does not have this problem, since the high-enthalpy flow is never stagnated. To examine the effects of dissociated test gas on combustion, a combustor model tested earlier in the HYPULSE facility at GASL was tested in T5.

The test conditions were chosen to correspond to a flight Mach number of 17. Experiments were conducted at two different pressure levels of the test gas entering the combustor model. Tests at the lower pressure (18.3 kPa) condition were designed to allow a direct comparison with identical tests (with the same combustor model) in the NASA HYPULSE facility at GASL. Tests at the higher pressure of 43.9 kPa, which is about 2.5 times that achievable in the HYPULSE facility, are more representative of the actual flight-capable propulsive system for the range of stagnation enthalpies (approximately 15 MJ/kg) in these tests. Some of the tests in T5 were conducted with the injection of hot hydrogen, which was heated by a combustion-driven reflected shock tube.[4] Whereas the HYPULSE tests were conducted with cold, room-temperature hydrogen (T_t = 300 K), the shock-heated hydrogen (T_t = 1250 K) in the T5 tests allowed for a more realistic flight simulation. In a real flight situation, the use of hydrogen fuel to cool the combustor and vehicle prior to its injection into the combustion chamber, raises its stagnation enthalpy.

The combustor model is sketched in Fig. 1. It is rectangular in cross section with the dimensions of 50.8 by 25.4 mm and is 711 mm long. The injector is mounted flush with the lower wall, with the fuel being injected at an angle of 15 deg to the flow direction. The injector is located at a distance of 177 mm from the combustor inlet. The conditions at the combustor inlet and the exit conditions for the fuel injector are listed in Tables 1 and 2, respectively.

The experimental data analyzed in this study are given by Belanger.[5] The measured data consist of static pressure measurements on the lower (injector) and the upper (opposite) walls. Some flow visualization pictures were obtained using a differential interferometry system. To resolve the position and structure of the fuel plume, a resonant enhancement technique was used.

Analysis

The numerical code used in this study is the general aerodynamic simulation program (GASP), version 1.3.[6] Numerical predictions from this version of GASP have been systemati-

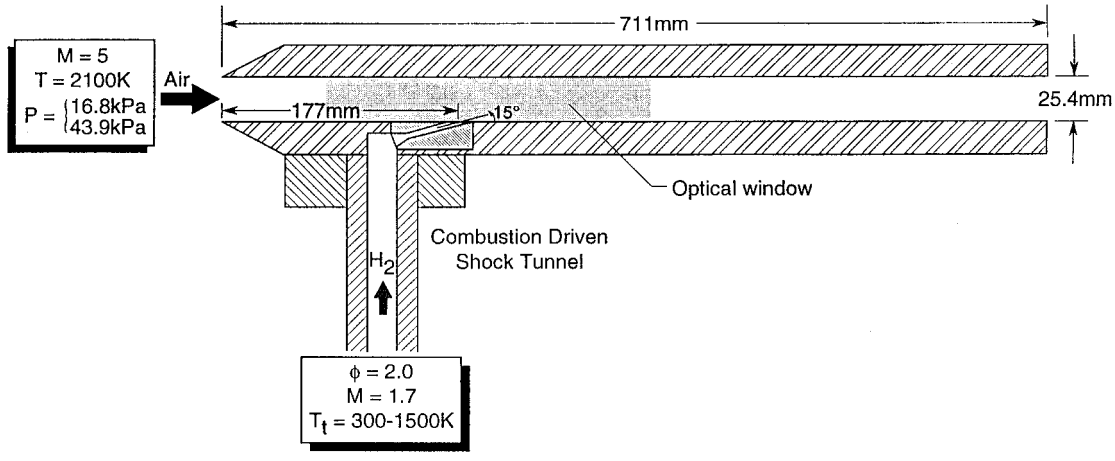

Fig. 1 Schematic of the combustor model.

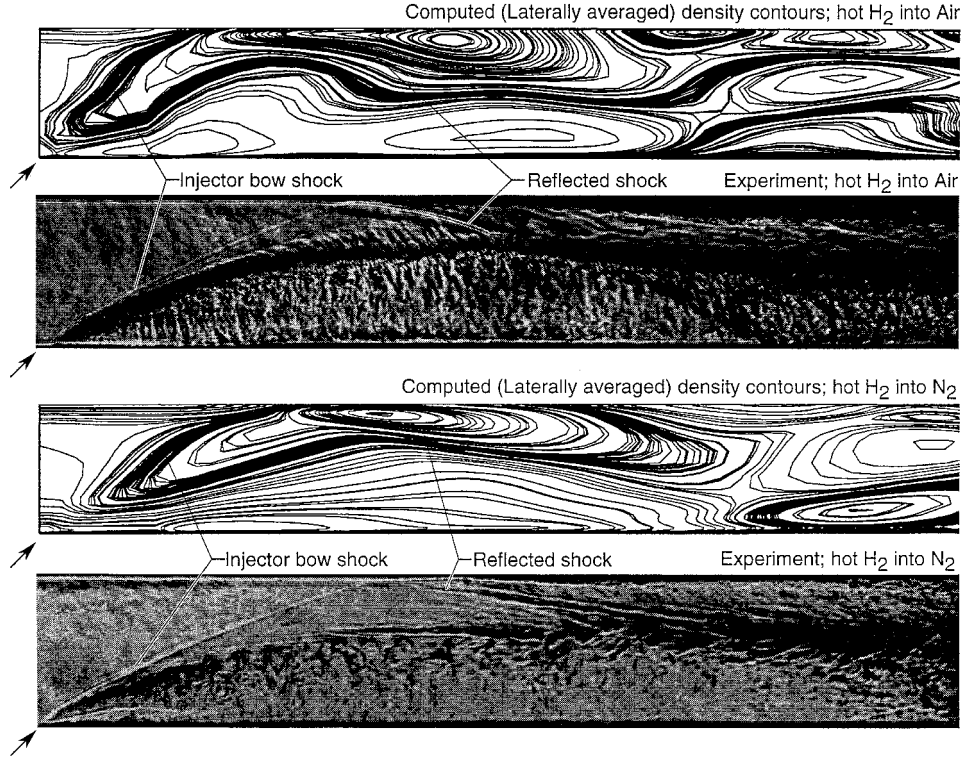

Fig. 2 Comparison of computed density contours with interferograms.

cally compared with available low- and high-enthalpy experimental results (as well as numerical predictions from the SPARK code) by Srinivasan et al.[7] For the low-enthalpy simulations, the predictions from GASP showed good agreement with the location of fuel core and the penetration and spreading of the fuel plume as observed in the experiments. However, these simulations did not show the same amount of fuel entrainment in the boundary layer as was inferred from images of the fuel using a laser-based fluorescence technique. For high-enthalpy flows, the results from GASP code were in agreement with the measured wall pressure.

The GASP code solves the full Reynolds-averaged, compressible form of the Navier–Stokes, energy, and species conservation equations and can be run in explicit, or implicit, space-marching or elliptic modes. Various upwind-based differencing schemes are also available. In GASP, the governing equations are discretized using a finite volume approach, and can be solved for one-, two-, or three-dimensional geometries. The code has several thermodynamic, turbulence, and chemistry models built into it. The specific choices made in this study are described in the following paragraphs.

The inviscid flux vectors were split following the approach described by Van Leer.[8] Flux limiters were used to limit the oscillations in the solution caused from discontinuities. Initial efforts revealed that reliable and stable solutions can be obtained by marching in the main flow direction, i.e., x direction. Thus, in all the results presented here, the parabolized form of the Navier–Stokes (PNS)[9] has been used. Since the flow is supersonic in the x direction, no flux splitting was employed in that direction. In all of the computations, the flow was taken to be turbulent from the leading edge, except for the tare case, in which a laminar flow model was used over the entire length of the combustor.

The viscosity of the mixture was computed using Wilke's semiempirical formulation, with the viscosity of each species being determined using Sutherland's law.[6] The thermal conductivity was modeled similarly. Turbulent interactions were modeled using the eddy viscosity model from Baldwin and Lomax,[10]

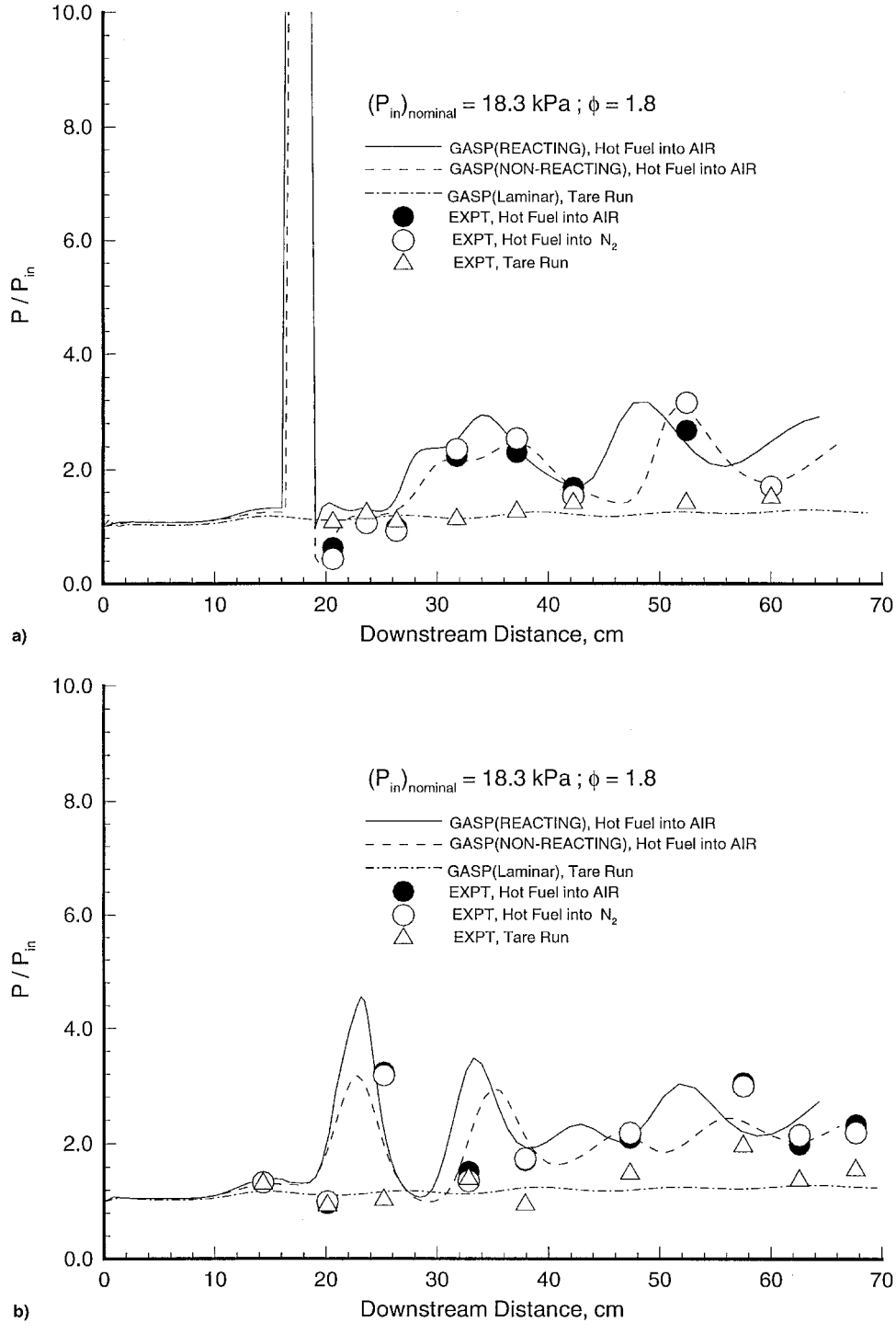

Fig. 3 Comparisons of CFD solution with mixing and reacting data: a) injection wall and b) opposite wall.

with the modifications from Goldberg.[11] Also, the turbulent viscosity was limited to 1000 times the local laminar viscosity to keep the level of diffusion within the jet structure within realistic physical bounds. However, this limiter was included primarily as a precautionary measure and did not affect the computations in any part of the flow. The turbulent Prandtl and Schmidt numbers were taken to be 0.9 and 0.5, respectively.

In this study, the finite rate chemical reaction of gaseous hydrogen and air was modeled by using the seven-species, seven-reaction model described by Drummond et al.[12] The seven species considered in the computations were N_2, O_2, H_2, OH, H_2O, H_1, and O_1. The presence of NO in the test gas was not explicitly accounted for since Jachimowski[13] has shown NO to be essentially inert at the pressure levels encountered in these tests. However, the amount of oxygen in NO was equally distributed between O_2 and O_1.

The governing equations were solved on a three-dimensional grid, which was highly compressed in the regions where high gradients exist. A simple exponential formula was used to cluster the grids in the high gradient regions. The grids were uniformly distributed in the region where fuel was injected. Fuel was injected at an angle of 15 deg to the main flow. Thus, the actual region on the lower wall of the combustor over which the fuel was injected was elliptical in shape. In the computations, this elliptically shaped region was modeled by a rectangle with the same area. The discharge coefficient was ac-

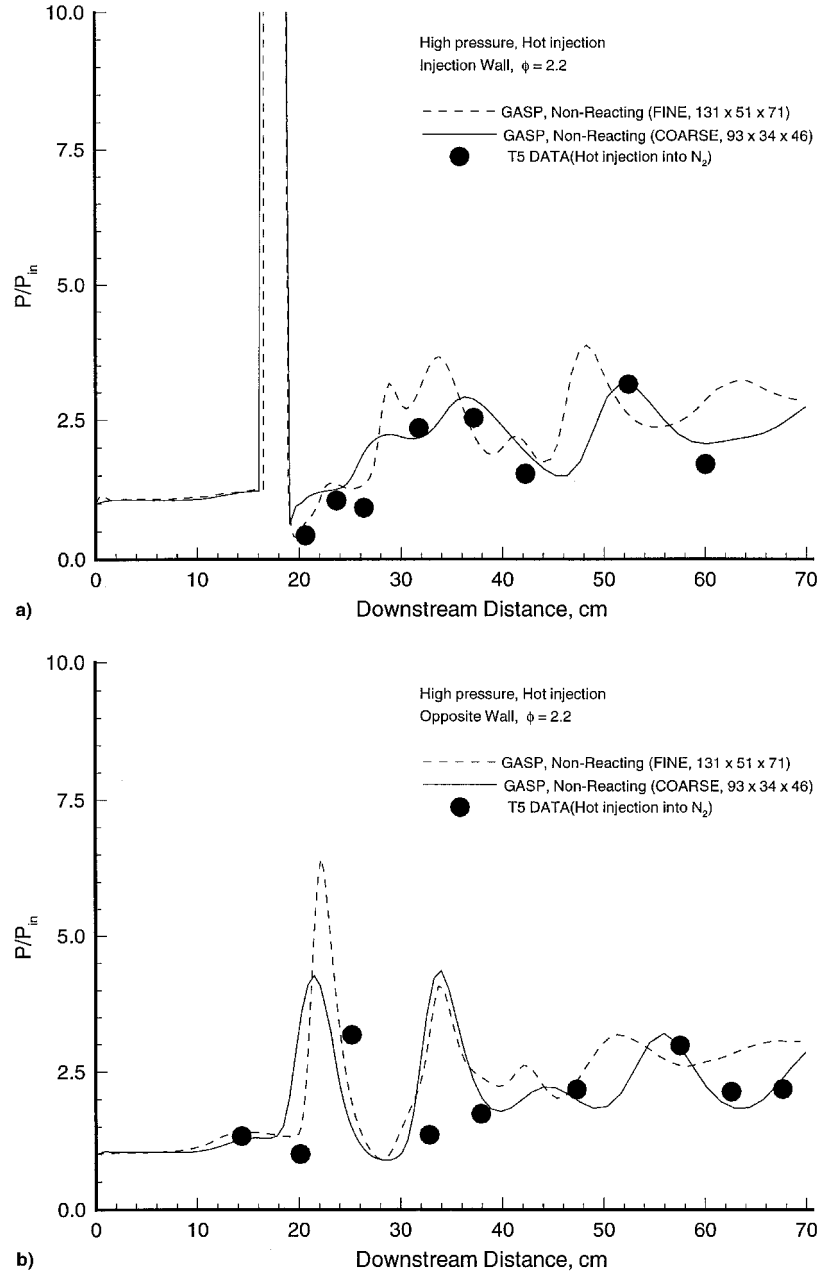

Fig. 4 Comparison of coarse and fine grid CFD solutions: a) injection wall and b) opposite wall.

counted for by a slight change in the exit pressure of the fuel jet. In simulations with a coarse grid, 93 × 34 × 46 nodes were used in the x, y, and z directions, respectively. For the fine grid, 131 × 51 × 71 nodes were used.

The inflow boundary was supersonic, and so the velocities, static temperature, static pressure, and species concentration were specified and fixed there. No-slip conditions were enforced on all of the solid boundaries. The vertical plane passing through the centerline of the lower wall of the combustor (as well as the centerline of the injector) was taken to be a plane of symmetry. In view of the small test flow times encountered in the T5 reflected-shock tunnel (1–2 ms), all of the solid walls were taken to be at a constant temperature of 300 K.

Results and Discussion

Based on the procedure outlined earlier, the GASP code was applied to compute the flow through the combustor model (Fig. 1) for the conditions listed in Tables 1 and 2. The time-varying form of the governing equations was integrated until convergence to a steady state was obtained. Results of the GASP calculation are presented and discussed in this section in terms of three issues. First is the general level of agreement of the experimental data with the computations. There were two sources of experimental data: 1) flow visualization images and 2) measured static pressure distributions on the lower (injection) and upper (opposite) walls of the combustor. The second issue involves the effect of fuel temperature, i.e., comparison of the results with hot and cold fuel injection. The third issue is a comparison between low- and high-pressure results, both with hot hydrogen injection. The experimental data as well as the numerical computations involve three categories of flows. In a tare run there is no injection, whereas in a mixing run there is injection of hydrogen into a nitrogen main stream, and in a combustion run there is injection of hydrogen into air.

Data–CFD Comparisons

Figure 2 shows a comparison between the flow visualization photographs and the computed density contours (laterally averaged) for the high-pressure case. The bow shock caused from

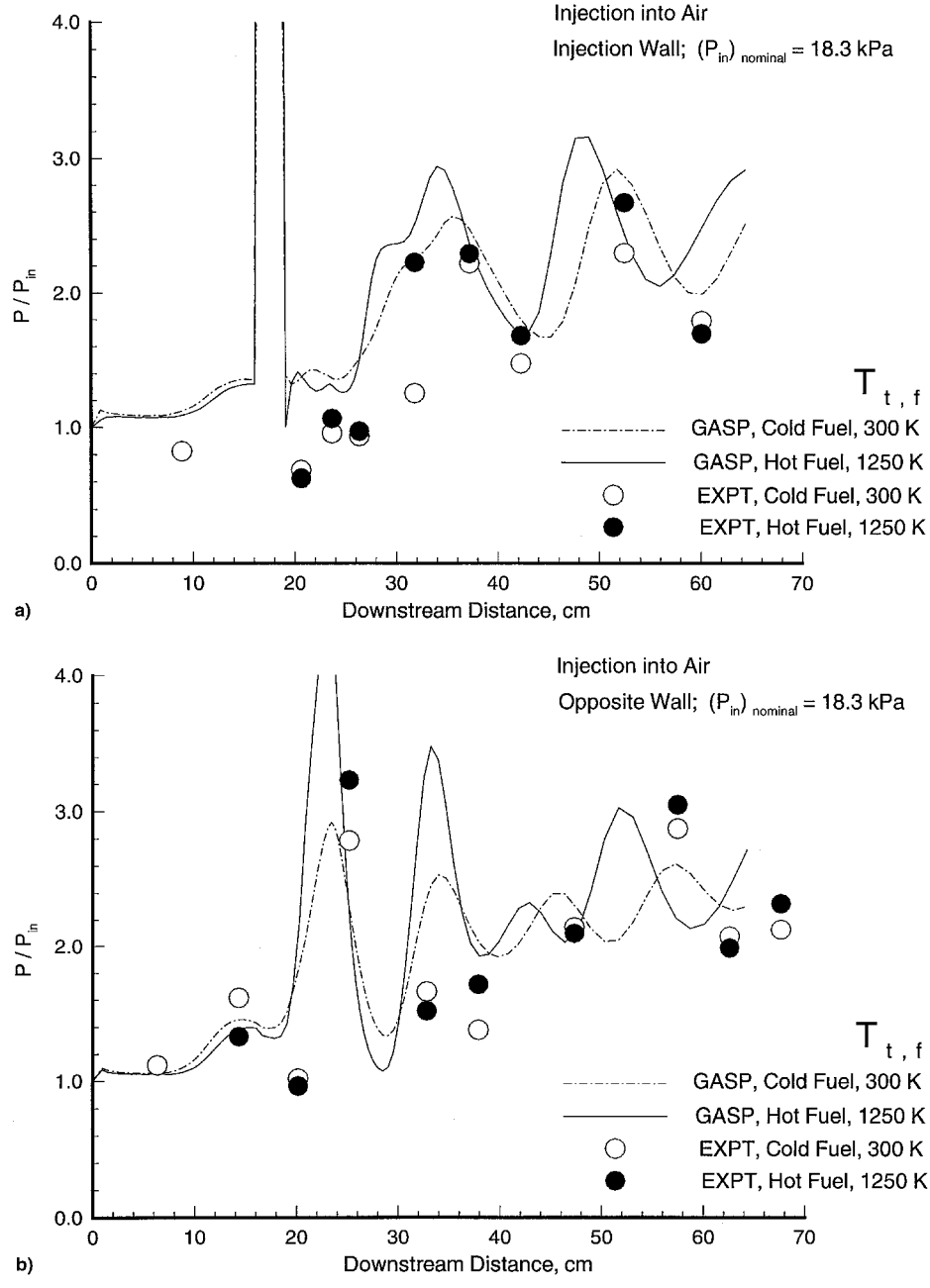

Fig. 5 Effect of hot/cold injection on centerline static pressure distribution: a) injection wall and b) opposite wall.

the injector and its reflection from the opposite wall are captured in the computations. The interferograms do not show any recirculation near the injector, which clearly justifies the use of the marching (PNS) algorithm in this study.

The low-pressure experiments in T5 were designed to provide a database for comparison with identical tests done in the HYPULSE facility. Belanger[5] has given a detailed comparison of the static pressure distributions measured in the two facilities. The general level of agreement is excellent. These comparisons show that the flow entering T5 is free from the large localized pressure disturbance that affected the data in HYPULSE in the region upstream of the injector.

Figures 3a and 3b show the downstream variation of the centerline static pressures on the lower and upper walls of the combustor, respectively. Experimental data from tare, mixing, and combustion experiments are compared with corresponding computed results, under low-pressure conditions, at $\phi = 1.8$. Here, ϕ is the hydrogen–air equivalence ratio. The agreement between the data and computations is seen to be quite good. The oscillations in the wall pressure as the flow proceeds downstream result from the reflections of the bow shock from the walls of the duct. In the region near the injector, the computations with a reactive flow model show a significantly higher pressure compared with mixing calculations. This results from the combustion that takes place in this region. Additional evidence for this inference can be found in the experimental flow visualization images in Fig. 2. From the interferograms of the experiments with air and nitrogen, it is seen that the bow shock in the case of air is shifted further to the left compared to its location in the case of nitrogen. This implies a significant level of combustion in the bow shock region. However, comparisons of the mixing (nonreacting) and reacting flow results over the remainder of the flow region, show that pressure rise to be practically the same for both. Thus the effect of heat release caused by combustion is essentially to shift the shock system and not to affect the pressure signature on the walls. This result is primarily a consequence of the high total enthalpy of the test gas. A secondary cause is the high static temperature of the test gas, which results in more dissociation than combustion product formation. Simi-

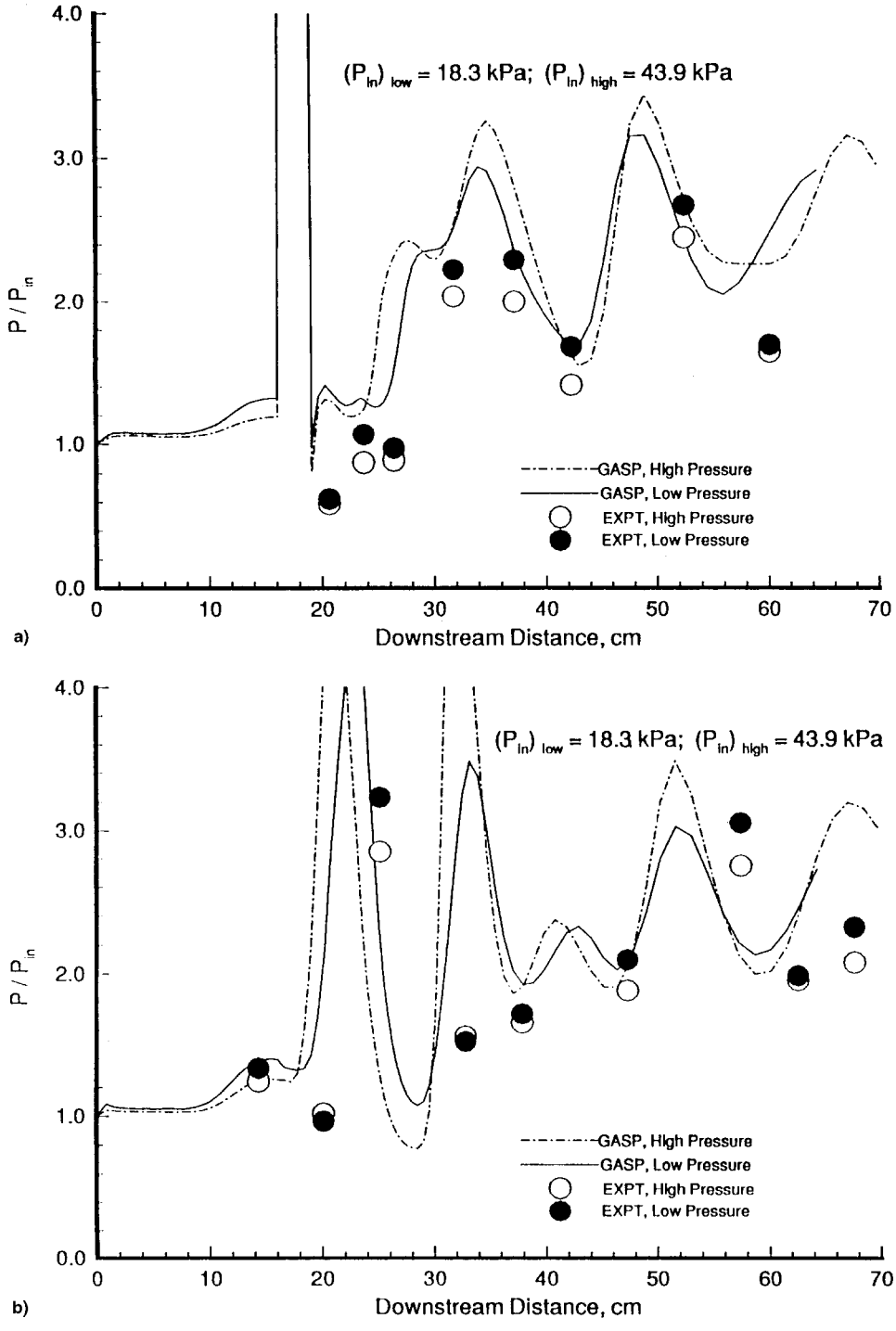

Fig. 6 Effect of test gas pressure on centerline static pressure distribution: a) injection wall and b) opposite wall.

lar conclusions have been reported by Bobskill et al.[14] and Srinivasan et al.[7] in their analyses of data from the NASA HYPULSE facility.

All of the results discussed so far were obtained with a coarse grid. In Figs. 4a and 4b a comparison is shown between results for the wall pressure distributions in a mixing case obtained with coarse and fine grids. While there is a difference between the computational predictions with the two different grids, the level of agreement with the experimental data is about the same for either grid. In view of this, all of the remaining results reported here were obtained with a coarse grid. Also note in this study that wall parameters (whose accurate prediction requires a fine grid) such as wall heat flux were not of primary interest since these were not measured in the tests.

Effect of Fuel Temperature

The effect of fuel temperature, characterized by its value at the injector exit, on the wall pressure is illustrated in Figs. 5a and 5b at the low-pressure condition for air at $\phi = 1.8$. The effect of the hot fuel is to cause stronger shocks, which result in higher pressures. However, the stronger shocks with the hot fuel injection result from the larger injection pressure that was required to match the value of ϕ, with that for cold injection. Also, with hot fuel injection, the general temperature level of the flow is raised, causing a decrease in the local Mach number levels (resulting from an increase in the speed of sound), which in turn causes steeper shock angles. This is evident from Figs. 5a and 5b where the peaks in wall pressure for the hot injection case are shifted to the left compared to cold injection results.

A comparison of the injectant mass fraction contours in the crossflow plane (not shown) did not show any significant differences in the spreading of the fuel plume for these hot and cold injection cases.

Pressure Effect

Figures 6a and 6b show the effect of varying the stream pressure on the wall static pressure. The computed results indicate a trend of wall pressure increasing with increasing inlet stream pressure. This observation can be attributed to the expected increase in the rates of chemical reaction with increasing pressure level. However, the experimental data seem to imply the opposite trend. But the differences between the high- and low-pressure experimental data are within the limits of measurement error. It can therefore be reasonably concluded that for the conditions of these tests, with hot fuel injection, high and low stream pressures result in similar wall distributions. Thus, for the conditions of these tests, varying the inlet stream pressure has a smaller effect compared to that observed by varying the fuel temperature.

Performance Parameters

The primary objective of using an injector is to deliver fuel so that a desired level of mixing of fuel and air can be achieved over the length of the combustor. It is well known that at high Mach numbers, rates of mixing are inherently lower.[15] Thus, at the high Mach number range characteristic of transatmospheric flight, mixing of fuel and air in the combustor is a critical issue for an air-breathing vehicle. Comparisons of the performance of the injector will be made in terms of two parameters: 1) mixing and 2) combustion efficiencies. Mixing efficiency is a number between 0–1 and is defined as the fraction of the least available reactant that can undergo complete reaction, without further mixing. Combustion efficiency is the fraction of the least available reactant that has reacted completely. Mixing efficiency represents an upper bound for the combustion efficiency.

At each cross-sectional plane η_m is computed as

$$\eta_m = \frac{\int_{A_c} \rho u Y_R \, dA}{\dot{m}_R}$$

The denominator is the axial flow rate of reactable fuel based on the overall ϕ. Thus, it represents the maximum value of the axial flow rate of reactable fuel at any location downstream of the injector. If the overall ϕ is greater than unity, $\dot{m}_R = f\dot{m}_{air}$. If the overall $\phi < 1$, then $\dot{m}_R = \dot{m}_{fuel}$. The numerator represents the computed axial flow rate of reactable fuel at a given downstream location. In the computational cells in the cross-plane that are fuel rich, $Y_R = f(1 - Y_{fuel})$. In the cells that are fuel lean, $Y_R = Y_{fuel}$. In computing the combustion efficiency, a formula identical to that for η_m is used with Y_R in the numerator replaced by the mass fraction of hydrogen in the form of water. Thus, η_c is computed as

$$\eta_c = \frac{\int_{A_c} \rho u Y_{H_2O} \left(\frac{\tilde{M}_{H_2}}{\tilde{M}_{H_2O}}\right) dA}{\dot{m}_R}$$

Here, $\tilde{M}_{H_2}$ and $\tilde{M}_{H_2O}$ are the molecular weights of hydrogen and water, respectively. Thus, the numerator in the combustion efficiency represents the axial flow rate of the reactable fuel that has undergone complete combustion. The definition of $\dot{m}_R$ is the same as that in η_m.

The performance characteristics of the combustor are shown in Figs. 7 and 8. In Fig. 7, a comparison between the results with hot and cold injection is illustrated. Clearly, the mixing and combustion efficiencies are higher with cold injection. This can be attributed to the higher main stream to jet velocity ratio for the cold injection case. From Fig. 8, it is clear that high-pressure results in higher mixing and combustion efficiencies. This principally results from the larger amount of fuel injected in the high-pressure case ($\phi = 2.2$) compared with the low-pressure case ($\phi = 1.8$). From Figs. 7 and 8 it is clear that in the near field (region close to the injector), there is a rapid rise in the mixing efficiency, followed by a more gradual rise in the far-field region. The oscillations observed in the mixing efficiency over the length of the combustor correlate with the location of reflected shocks in the flow region. These features are consistent with the results presented in Refs. 7 and 14.

An important issue associated with mixing is the penetration of the airstream by the fuel jet. Earlier experiments concerned with penetration of normally injected[16] and angled jets[17] indicated that the depth of penetration increases (nonlinearly) with R. Penetration of the fuel jet under typical injection and pressure conditions considered in this study can be discerned from the plots of the distribution of hydrogen concentration in the

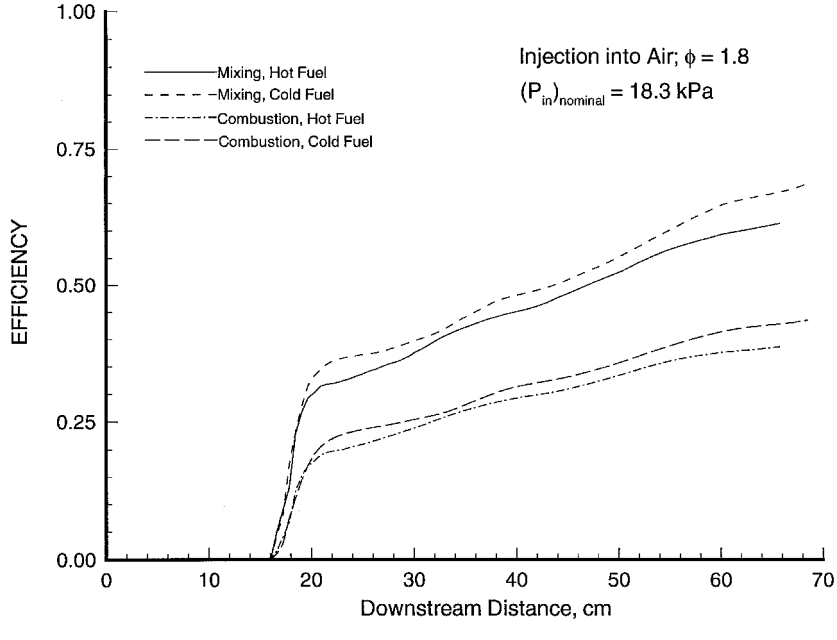

Fig. 7 Variation of mixing and combustion efficiencies: hot vs cold injection.

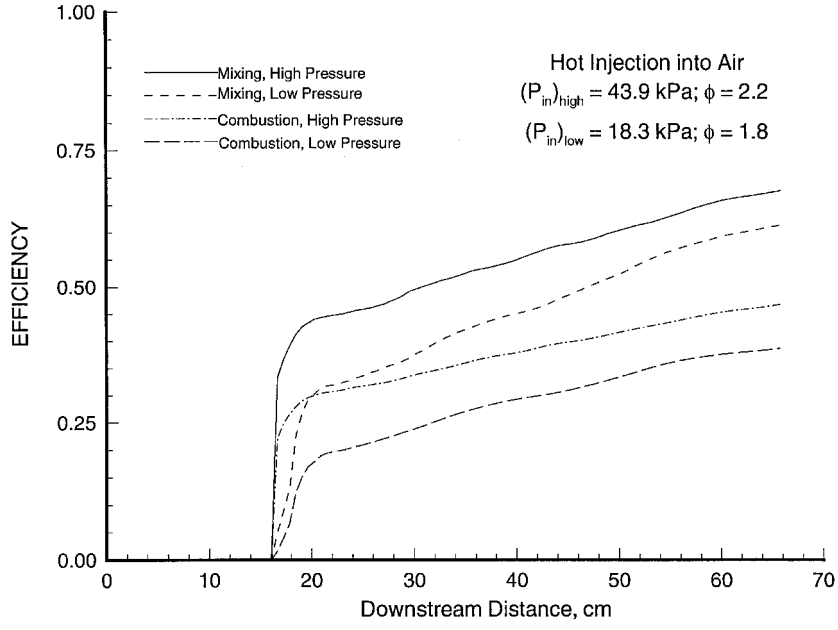

Fig. 8 Variation of mixing and combustion efficiencies: high vs low pressure.

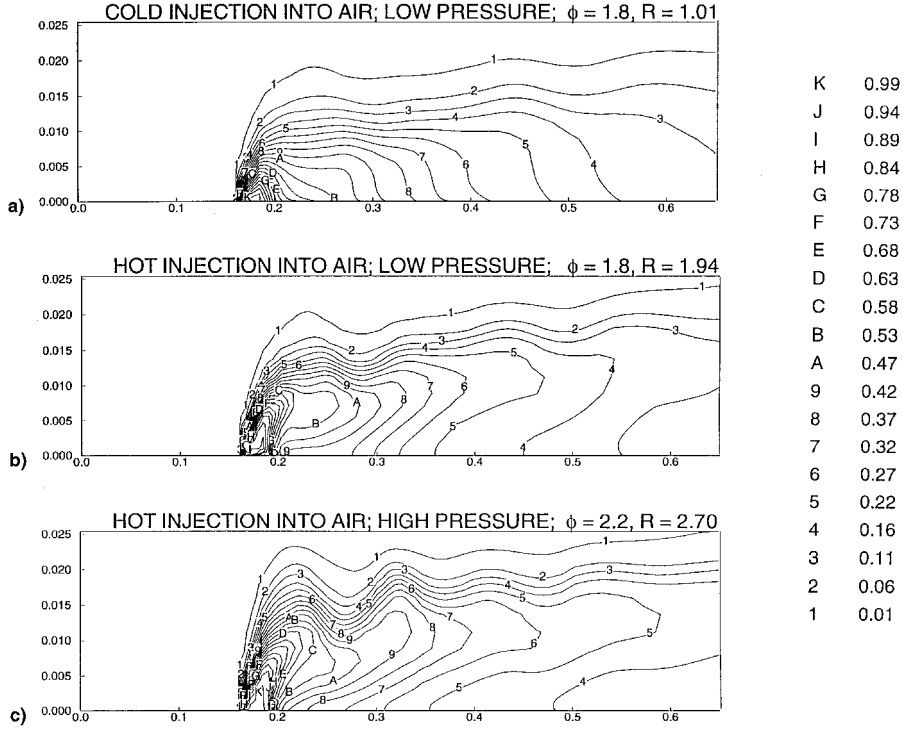

Fig. 9 Comparison of the distribution of injectant mass fraction in the plane of symmetry.

x–z plane (plane of symmetry) shown in Fig. 9. At low pressure, a hot hydrogen jet (R = 1.94) is seen to penetrate farther into the airstream than a cold jet (R = 1.01). Also, with hot injection, a higher pressure (R = 2.70) results in better penetration, contributing to the better mixing observed in Fig. 7. Thus, these new results are in qualitative agreement with established correlations on jet penetration. It is interesting to note from Fig. 7 that at low-pressure conditions, cold injection resulted in higher mixing efficiency compared with the hot injection case. From Fig. 9 it can be seen that, at low pressure, the hot jet penetrates slightly farther than the cold jet. Clearly, an increased jet penetration does not always imply an increased mixing efficiency. It can also be seen from Fig. 9a, that the cold jet loses its jet structure quite rapidly, indicating a relatively more vigorous mixing with the airstream. This enhanced mixing results from the larger value of the freestream to jet velocity ratio for the cold jet (2.7) compared with that for the hot jet (1.3).

Spatial Uniformity

An issue related to the mixing of hydrogen with the airstream is the spatial uniformity of the resulting mixture. In particular, it is of interest to assess the changes in the uniformity of the mixture (in the crossflow plane) downstream of the injection location. A measure of the deviation from uniformity, at a given downstream location, is the parameter C_{rms}, which is defined as

$$C_{\text{rms}} = \sqrt{\sum_{N} (C_i - \bar{C})^2 \Big/ N}$$

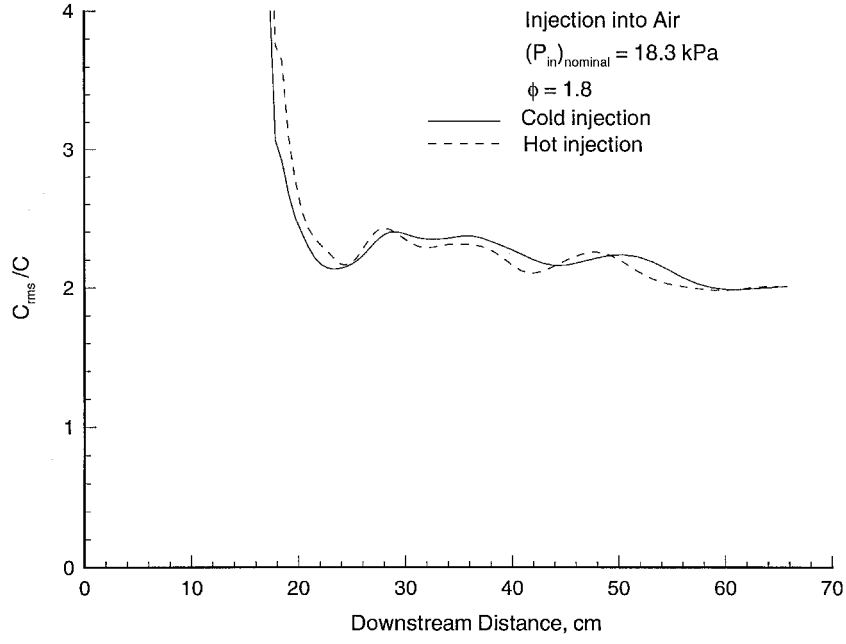

Fig. 10 Downstream decay of spatial nonuniformity of the injectant.

$$\bar{C} = \sum_{N} \frac{C_i}{N}$$

Here, C_i is a measure of concentration of hydrogen in the ith cell, and $\bar{C}$ is the average value with N being the total number of cells in the crossflow plane, at that downstream station. For a mixture with uniform composition, $C_{rms} = 0$. This particular choice of variables to characterize spatial uniformity is based on the theoretical approach of Briedenthal et al.[18] for incompressible flow. To account for the compressible and reactive nature of the flow, C_i was defined as

$$C_i = \dot{m}_{f,i}/\hat{m}_R, \qquad \hat{m}_R = \dot{m}_R/N$$

Here, $\dot{m}_{f,i}$ is the axial mass flow rate of the fuel for the ith cell in the crossflow plane. The term $\dot{m}_R$ is the same as that in the definition of η_m and represents the axial flow rate of the reactable fuel at a given downstream location. Associated with this definition of C_i, quantities $\bar{C}$ and C_{rms} can be defined; then, $\bar{C}$ would become equal to ϕ. Since $\hat{m}_R$ represents the mass flow rate of reactable fuel for any cell in the crossflow plane, a uniform fuel distribution would imply that C_i for any cell is equal to ϕ with $C_{rms}/\bar{C}$ becoming zero. For the results displayed in Fig. 10, this is not the case. Toward the exit of the combustor, the ordinate has decayed only to a value of 2, indicating that the distribution of fuel is still nonuniform. However, the decreasing trend in the value of the ordinate indicates that the mixture composition is progressing toward a uniform distribution. Plots of $C_{rms}/\bar{C}$ for both hot and cold jets are similar.

In Fig. 10, in the region close to the injector, there is a sharp drop in C_{rms}. Note that $\bar{C}$ being equal to ϕ does not vary with downstream location. A comparison with Fig. 7 shows that over the same region, the mixing efficiency increases rapidly. Also, downstream of this region, the mixing efficiency increases gradually and C_{rms} decreases rather gradually. Thus, these results indicate a correlation between mixing efficiency and spatial uniformity of the mixture.

Conclusions

A principal objective of this numerical investigation was to analyze the data for hydrogen injection into a hypervelocity flow in the pulse facility T5 at the Graduate Aeronautical Laboratories at GALCIT. Numerical results obtained with the GASP code showed good agreement with the measured static pressure distributions on the combustor walls. Also, the flow structure predicted by the numerical solution agreed with that inferred from flow visualization images. Additionally, the numerical solutions have provided information on the combustion and mixing efficiencies that could not be measured in the experiments. Two unique features of the data from T5 were the measurements done with hot hydrogen and those done at a pressure level of 0.5 bar. As expected, combustion efficiency was higher at the higher pressure level compared with that observed at the lower pressure level in the tests at T5 and in the previous tests at the NASA HYPULSE facility. Also, the mixing performance with hot hydrogen fuel is consistent with established correlations for scramjet design, which were based entirely on data from cold hydrogen injection tests. The issue of uniformity of the air–hydrogen mixture and its relation to the mixing efficiency has also been considered.

Acknowledgments

Krishnamurthy and Tiwari acknowledge the partial support for this work from NASA Langley Research Center through Grant NAG1-363. The work was initiated during Krishnamurthy's tenure as a NASA–American Society for Engineering Education Summer Faculty Fellow. Some of the work reported in this revised version was accomplished through support from Grant NAGW-2924 to North Carolina A&T State University. R. Krishnamurthy would also like to thank Shivakumar Srinivasan (Analytical Services & Materials, Hampton, Virginia) for his invaluable help with the use of GASP. Thanks also go to G. Y. Anderson, Head of the Hypersonic Air Breathing Propulsion Branch, and A. Auslender, Lockheed Engineering and Science Company, Hampton, Virginia, for their suggestions and discussions related to the issue of approach to uniformity of the mixture composition.

References

[1]Hornung, H. G., "Performance Data of the New Free-Piston Shock Tunnel at GALCIT," AIAA Paper 92-3943, July 1992.

[2]Tamagno, J., Bakos, R., Pulsonetti, M., and Erdos, J., "Hypervelocity Real Gas Capabilities of GASL's Expansion Tube (HYPULSE) Facility," AIAA Paper 90-1390, June 1990.

[3]Maus, J., Laster, M., and Hornung, H., "The G-Range Impulse

Facility — A High-Performance Free-Piston Shock Tunnel," AIAA Paper 92-3946, July 1992.

[4]Belanger, J., and Hornung, H. G., "A Combustion Driven Shock Tunnel to Complement the Free Piston Shock Tunnel at GALCIT," AIAA Paper 92-3968, July 1992.

[5]Belanger, J., "Studies of Mixing and Combustion in Hypervelocity Flows with Hot Hydrogen Injection," Ph.D. Dissertation, California Inst. of Technology, Pasadena, CA, April 1993.

[6]Walters, R. W., Slack, D. C., Cinella, P., Applebaum, M., and Frost, C., "A User's Guide to GASP," NASA Langley Research Center, Hampton, VA/Virginia Polytechnic Inst. and State Univ., Blacksburg, VA, Revision 0, 1990.

[7]Srinivasan, S., Bittner, R. D., and Bobskill, G. J., "Summary of the GASP Code Application and Evaluation Effort for Scramjet Combustor Flowfields," AIAA Paper 93-1973, June 1993.

[8]Van Leer, B., "Flux Vector Splitting for the Euler Equations," *Lecture Notes in Physics*, Vol. 170, Springer–Verlag, Berlin, 1982.

[9]Anderson, D. A., Tannehill, J. C., and Pletcher, R. H., *Computational Fluid Mechanics and Heat Transfer*, Hemisphere, New York, 1984.

[10]Baldwin, B. S., and Lomax, H., "Thin Layer Approximation and Algebraic Model for Separated Turbulent Flows," AIAA Paper 78-257, Jan. 1978.

[11]Goldberg, U. C., "Separated Flow Treatment with a New Turbulence Model," *AIAA Journal*, Vol. 24, No. 10, 1986, pp. 1711–1713.

[12]Drummond, J. P., Rogers, R. C., and Hussaini, M. Y., "A Detailed Numerical Model of a Supersonic Reacting Mixing Layer," AIAA Paper 86-1427, June 1986.

[13]Jachimowski, C., "An Analysis of Combustion Studies in Shock Expansion Tunnels and Reflected Shock Tunnels," NASA TP 3224, July 1992.

[14]Bobskill, G., Bittner, R. D., Riggins, D., and McClinton, C., "CFD Evaluation of Mach 17 HYPULSE Scramjet Combustor Data," AIAA Paper 91-5093, Dec. 1991.

[15]Papamoschou, D., and Roshko, A., "Observations of Supersonic Free Shear Layers," AIAA Paper 86-0162, Jan. 1986.

[16]Rogers, R. C., "A Study of the Mixing of Hydrogen Injected Normal to a Supersonic Airstream," NASA TND-6114, March 1971.

[17]McClinton, C. R., "The Effect of Injection Angle on the Interaction Between Sonic Secondary Jets and a Supersonic Free Stream," NASA TND-6669, Feb. 1972.

[18]Briedenthal, R. E., Tong, Kwok-On, Wong, G. S., Hamerquist, R. D., and Landry, P. B., "Turbulent Mixing in Two-Dimensional Ducts with Transverse Jets," *AIAA Journal*, Vol. 24, No. 11, 1986, pp. 1867–1869.